The Impact of Alumina Availability on Sulfate Resistance of Slag Composite Cements

Mark Whittaker[a,b], Maciej Zajac[c], Mohsen Ben Haha[c], Leon Black[b†],
[a]University of Aberdeen, King's College, Aberdeen, AB24 3FX, United Kingdom
[b]University of Leeds, Woodhouse Lane, Leeds, LS2 9JT, United Kingdom
[c]Heidelberg Technology Center GmbH , Rohrbacher Str. 95, 69181 Leimen, Germany
†Corresponding Author

Abstract

Slag cement pastes prepared with either 40% or 70% of slags by weight were prepared (W/B = 0.5) and subsequently exposed to a 3 $g.L^{-1}$ Na_2SO_4 solution. The slag cements were shown to be more resistant. Initially, ettringite levels rose, then plateaued upon carbonate AFm consumption, although monosulfate was also found to be in equilibrium with ettringite when using an Al-rich slag. Portlandite was initially consumed, to form ettringite, but leached out after prolonged attack until it was fully depleted, or nearly, with subsequently C-A-S-H being decalcified. Any excess aluminium released by the slag was bound to a calcium deficient C-A-S-H phase and hydrotalcite, sheltering the aluminates from ingressing sulfates. Mass balance further revealed that, if the slag in the blends were to fully dissolve to form C-A-S-H and hydrotalcite, there would have been insufficient aluminium and calcium to combine with sulfates to form ettringite. Rather, calcium from C-A-S-H would have continuously leached, leaving behind a silicate skeleton.

Key Words: Sulfate Attack, Cement, Slag, Characterisation, Durability

1 Introduction

External sulfate attack encompasses a series of interactions occurring within the cement matrix as sulfates percolate through it [1]. The sulfates react with available aluminium, and calcium, to

convert AFm hydrates to ettringite $C_6A\bar{S}_3H_{32}$ and, under extreme circumstances, portlandite to gypsum [2, 3, 4].

It is commonly believed that the formation of ettringite and gypsum, from monosulfate and portlandite respectively, are expansive reactions which are the cause the damage. [5, 6]. Still, ettringite precipitation alone cannot explain the damage caused by sulfate attack, and the link between ettringite formation and expansion is not clear [7, 8]. Rather, damage is caused when the expansive ettringite forms in pores small enough to exert a force on the matrix [3, 8, 9, 10, 11]. Furthermore, Yu proposed that the failure mechanism of mortars bars of slag blends exposed to sodium sulfate solution is dominated by the loss of surface material rather than a generalized expansion, as for plain Portland cement [12].

The replacement of cement with slag has previously been recognized as imparting sulfate resistance, particularly at higher levels of replacement [13, 14, 15, 16, 17]. Although the overall aluminium content is higher in a slag cement blend, it does not imply that more aluminium is readily available to react with sulfates. Such systems produce a C- S-H phase with a lower Ca/Si ratio [18, 19, 20], thus allowing aluminium incorporation within the phase. A hydrotalcite like phase is also common, binding aluminium. This restricts the amount of free aluminium which would react freely otherwise with sulfates [14, 21]. However, it has been seen previously [22] that alumina still promotes AFm formation at early ages, which may in turn convert to ettringite during attack, worsening resistance. Furthermore, not all of the available alumina goes to form ettringite. Fernandez-Altable has previously observed the formation of monosulfate by the end of their testing period [21].

The role of calcium in sulfate attack cannot be ignored either. Slags are typically calcium deficient compared to cement, therefore lowering the total calcium content of slag cements. A recent study

47 by Kunther et al. [23] found that the crystallisation pressure related to ettringite growth is reduced
48 when the Ca/Si of the C-A-S-H phase is lower.

49 This study investigates further the impact of alumina content in slag and calcium content in
50 composite cement on sulfate resistance, closely following the changes in hydrate composition
51 and amounts.

52 2 Materials

53 A CEM I 42.5 R, conforming to EN 197-1:2011, was chosen for this study along with two ground
54 granulated blast furnace slags differing in composition. The oxide composition of the raw
55 materials is shown in table 1.

56 **Table 1 Compositions of The Raw Materials, Determined by XRF (% Weight)**

		CEM I	Slag B	Slag C
LOI 950 °C	%	2.62	(+0.85)*	(+1.57)*
SiO_2	%	19.2(1)	39.7(5)	34.3(5)
Al_2O_3	%	5.5(0)	7.3(6)	12.3(3)
TiO2	%	0.2(7)	0.2(5)	0.9(3)
MnO	%	0.0(4)	2.5(4)	0.4(0)
Fe_2O_3	%	2.7(7)	1.3(3)	0.5(2)
CaO	%	62.2(8)	38.1(8)	38.4(9)
MgO	%	2.1(9)	7.6(5)	9.5(8)
K_2O	%	0.9(3)	0.6(5)	0.4(8)
Na_2O	%	0.0(8)	0.1(3)	0.2(4)
SO_3	%	3.1(0)	1.8(3)	2.6(1)
P_2O_5	%	0.1(7)	0.0(1)	0.0(1)
Total	%	99.15	99.69	99.93
Amorphous	%	-	99.0	98.3
Mg/Al		-	4.74	3.52

*The sample was oxidized with HNO_3 before determination of LOI

57

58 Compared to CEM I, the slags were characterised by being deficient in calcium, and richer in silica,
59 magnesium, and aluminium. The slags were chosen to emphasize the role of aluminium content

on sulfate resistance. As such, slag C (12.33%) was richer in aluminium than slag B (7.36%). Similarly, slag C was richer in magnesium and calcium than slag B. However, the Mg/Al molar ratio of the slag was lower than for slag B. The mineralogical composition of the CEM I used is shown in Table 2. The CEM I was compromised of primarily of C_3S and C_2S. The cement was contained moderate amounts of aluminium in the form of C_3A (7.5 %) and C_4AF (8.3 %). The total calcium sulfate content, as anhydrite and hemihydrate, totaled 4.4 %.

Table 2 Mineralogical Composition of CEM I

Phases		CEM I
C_3S	%	61.0
β-C_2S	%	11.9
C_3A	%	7.5
C_4AF	%	8.3
Calcite	%	3.7
anhydrite	%	2.9
Hemihydrate	%	1.5
other	%	3.2

3 Methods

Pastes were used to assess sulfate resistance, according to the mix designs shown in Table 3. The specimens were prepared by replacing either 40% or 70% of the cement by weight with slag. A further blend, containing 3% additional anhydrite by weight, was prepared using slag C at 40% replacement. Note, the overall SO_3 content accounts only for that supplied by the clinker and the added anhydrite.

Table 3 Mix Design of all Blends

	C_1	C_140S_b	C_140S_c	C_140S_c\$	C_170S_c
CEM I	1.00	0.60	0.60	0.58	0.30
slag	-	0.40	0.40	0.39	0.70
anhydrite	-	-	-	0.03	-
w/binder	0.50	0.50	0.50	0.50	0.50
w/cement	0.50	0.83	0.83	0.86	1.67
Final SO_3 in cement (%)	3.1	1.86	1.86	4.96	0.93

50 mm long 25mm diameter paste cylinders were prepared to assess any changes in microstructure during attack (figure 1). All samples were cured for a period of 14 days in water baths prior to exposure to a 3 $g.L^{-1}$ Na_2SO_4 solution, which was renewed fortnightly. The volume of the solution was four times that of the samples. The experimental setup was carried out in closed containers under ambient conditions (20°C) and no precautions were taken to prevent carbonation. The pastes were characterised by scanning electron microscopy (SEM) in backscattered electron mode, X-ray diffraction (XRD), thermal gravimetric analysis (TGA) and mercury intrusion porosimetry (MIP).

The samples in this study are referred to by their total curing time, and not by the time exposed to sulfates, e.g. a sample a 28 day sample has, in fact, only been in a sulfate bath for 14 days.

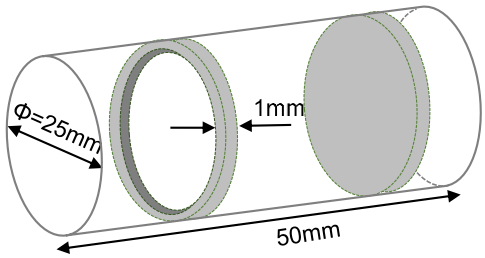

Figure 1 Schematic Drawing of the Paste Samples Prepared for Sulfate Attack

SEM analyses were conducted on pastes, from which transverse cuts were taken using a Struers Accutom-50 (Struers diamond cut-off wheel MOD 13). 2 mm thick cuts were taken near the middle of the sample, where the ingress of sulfates was radially unidirectional. The disks were freeze dried to constant weight and subsequently resin impregnated. The samples were polished using silicon carbide paper and any remaining scratches removed with diamond paste (down to 0.25 µm). Energy dispersive X-ray (EDX) point analyses were conducted on micrographs with a 130x97 µm field of view; a 12x12 grid point was set up and measurements were taken from the edge of the sample to a depth of 5 mm, at 0.5 mm intervals. Any measurement associated with

CH, anhydrous phases, and porosity was removed from the data. As such, the sulfate profile was measured and any changes in hydrate assemblage and composition were assessed. Further EDX point analysis was also performed on the slag hydration rims near the surface and at a depth of 5 mm.

X-ray diffraction (XRD) analysis was conducted on the outer 1 mm diameter of the pastes, cut along the length of a 5 mm long cylinder, 50 mm in diameter. The samples were crushed to a fine powder using a pestle and mortar and backloaded into a 16 mm diameter sample holder. Diffraction patterns were collected using a Philips Panalytical X'Pert MPD diffractometer equipped with a CuKα X-ray source operating at 40kV and 40mA, and an X'Celerator detector. Patterns were measured from 7 to 70 ^{o} 2θ with a step size of 0.0334 ^{o}. Rietveld refinement of the patterns was conducted using the Philip's X'pert HighScore Plus programme version 2.2a (2.2.1). The XRD patterns were individually fitted for each sample, to account for the amorphous phases. Quantification of the X-ray amorphous phase content was conducted using the external standard and G-factor methods [24], with corundum (Al_2O_3) serving as the standard. Reference files were taken from the ICSD library.

The portlandite (CH) content in the outer 1 mm of the pastes was determined, on freeze-dried paste samples, by thermal gravimetric analysis (TGA) analysis using a Stanton Redcroft 780 series under a nitrogen atmosphere, with a 20 °C/min heating rate from 20 to 1000 °C. The portlandite content was determined using the tangent method and normalised to the % mass at 550 °C.

$$\%\mathrm{CH} = \left(\frac{\mathrm{CH_w} \times \left(\frac{\mathrm{M_{CH}}}{\mathrm{M_H}} \right)}{\mathrm{W_{550}}} \right) \times 100$$

where:

CH_w – mass loss due to dehydration of CH
M_{CH} – molar mass of CH, 74 g.mol^{-1}
M_H – Molar mass of water, 18 g.mol^{-1}
W_{550} – % mass loss at 550 ° C

MIP measurements were performed using Micromeritics AutoPore IV device. The samples were prepared in the same way as for TGA, but without grinding.

Phase assemblage and total pore volume were modelled using GEMS (Gibbs Energy Minimisation) [25]. Thermodynamic data was taken from the PSI–GEMS database [26, 27] along with cement specific data [28, 29, 30]. Modelling was performed to assess the porosity of the systems after 14 days of hydration. The neat and slag cement compositions were defined in Table 2 and Table 3. The hydration degree of the clinker and slag components of the blends was taken from [22]. The porosity was calculated as the ratio between the volumes of any anhydrous phases remaining and hydrates at 14 days and the total initial volume of the pastes. Consequently, this takes into account any chemical shrinkage associated with cement hydration. Additionally, thermodynamic modelling was used to calculate the maximum supersaturation with respect to ettringite. A similar approach has been used previously [23]. A C–S–H portlandite system with a varying amounts of $Ca(OH)_2$ and SiO_2 was used to illustrate the development of the AFt saturation index for an increasing alumina concentration in the pore solution. The calculations were performed at two sulfate concentrations, 1 and 10 mM/L. About 30 mM/L NaOH was added to increase pH to values typical for real cements.

Porosity was assessed by means of scanning electron microscopy (SEM) observations in backscattered electron mode (SEM-BSE). 50 SEM-BSE images were collected per sample at a magnification of 800x and the porosity was assessed following a protocol previously used by Scrivener et al. [31]. From the greyscale histogram, an arbitrary pore threshold was taken as the intersection of the tangents of the first leg and that of the rising, left hand edge of the C-A-S-H peak. This method, however, does not allow to fix an unambiguous pore threshold, and an arbitrary value must be set [32].

4 Results

4.1 Microstructure prior to sulfate exposure

The hydration of the system under investigation under idealized curing conditions, i.e. immersion in a saturated lime solution, has been described previously [33]. After 14 days of curing, about 80 % of the cement in the blends had already reacted. In contrast, the degree of reaction of slags B and C were 37 % and 47 % respectively. As a result, the overall degree of hydration of the slag blends, defined as the combined degree of hydration of both the slag and cement component weighted by their respective mass fraction, was always lower compared to the neat cement. The slag blends, consequently, were characterized by having a higher total porosity (Figure 2).

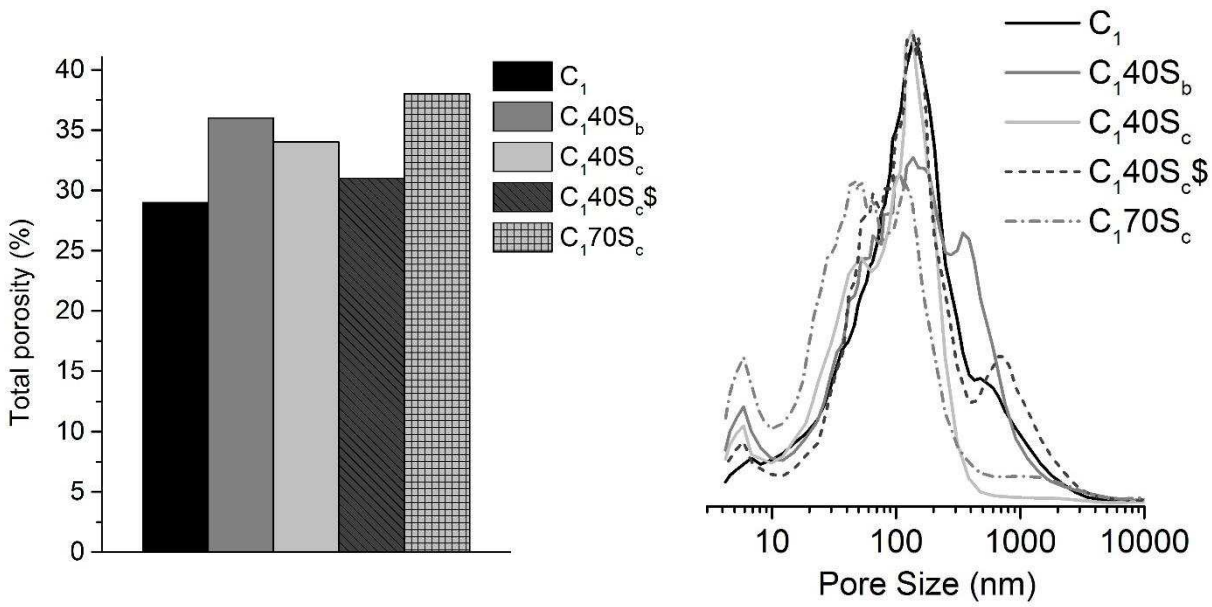

Figure 2 Total Porosity Calculated by Thermodynamic Modelling and Pore Size Threshold measured by MIP after 14 Days of Hydration

However, despite the higher total porosity, slag-cement blends were typically characterized by having a more refined porosity [34]. At 14 days the slag cements were characterized by having a similar or finer porosity compared to the neat cement. The pore structure was most refined in

blends C_140S_c and C_170S_c due to the higher reactivity of slag C. However, the addition of sulfates coarsened the porosity.

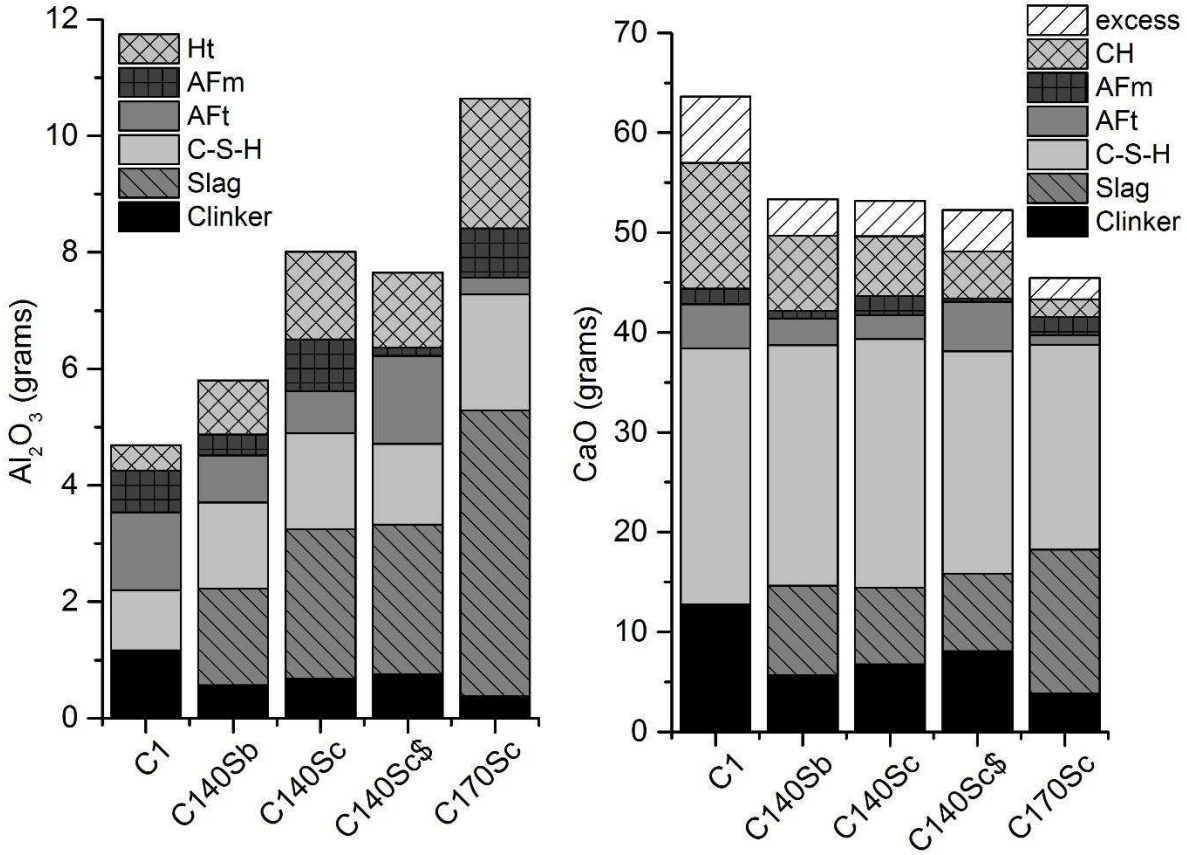

Figure 3 Alumina and Calcium Distribution after 14 Days of Hydration by Mass Balance. The composition of the C-A-S-H phase was taken from the reference values in Table 4.

The neat cement reacted with water to produce amorphous C-A-S-H, portlandite, ettringite and carbonate AFm hydrates. In the slag cements, hydrotalcite was also a dominant hydrate [33]. For the hydrotalcite phase, the Mg/Al was measured on pastes cured for 180 days when thick enough slag hydration rims were found for accurate measurements. The values varied from 1.93 for C_170S_c to 2.67 for C_140S_b [35]. For the neat system, a Mg/Al ratio of 2 was assumed. Figure 3 shows

the distribution of alumina and calcium in the aforementioned hydrates after 14 days of hydration, e.g. before the samples were exposed to external sulfate attack (which is important from the perspective of the formation of ettringite in the sulfate solutions). The distributions were assessed by carrying out mass balance calculations, and the methodology applied is described in the appendix. Combining TG, XRD and SEM analyses, the extent of the various hydration reactions was first assessed. Subsequently, the amounts and compositions of the hydrates were determined and the Al and Ca distributed accordingly. In the blends using Slag C without any added calcium sulfate, the amount of aluminium in AFm was greater than the amounts observed in the neat system. Conversely, less was observed when using a low alumina slag ($C_1 40 S_b$) or spiking the mix with calcium sulfate ($C_1 40 S_c \$$). It is interesting to note that, prior to attack, the amount of alumina in the carbonate AFm phases, that which is susceptible to form AFt, was either nearly matching or lower in the slag cements when compared to neat cement. However, it should be noted that AFm phases are partially XRD amorphous and therefore a comparison in peak intensity between two systems can be misleading; internal investigations seemed to suggest that the additional of slag improved the crystallinity of AFm hydrates. However, the addition of anhydrite in $C_1 40 S_c \$$ converted much of the available alumina to ettringite during the early stages of hydration. Note that, as mentioned before, even for the more reactive slag C, the degree of hydration was only 47%. Therefore, much of the alumina remained in unreacted slag.

The total calcium content of the composite cements was lower when compared to the pure cement (Table 1, Figure 3). This was reflected in the lower calcium hydroxide contents in the slag cements.

4.2 Physical Observations of Paste under Sulfate Attack

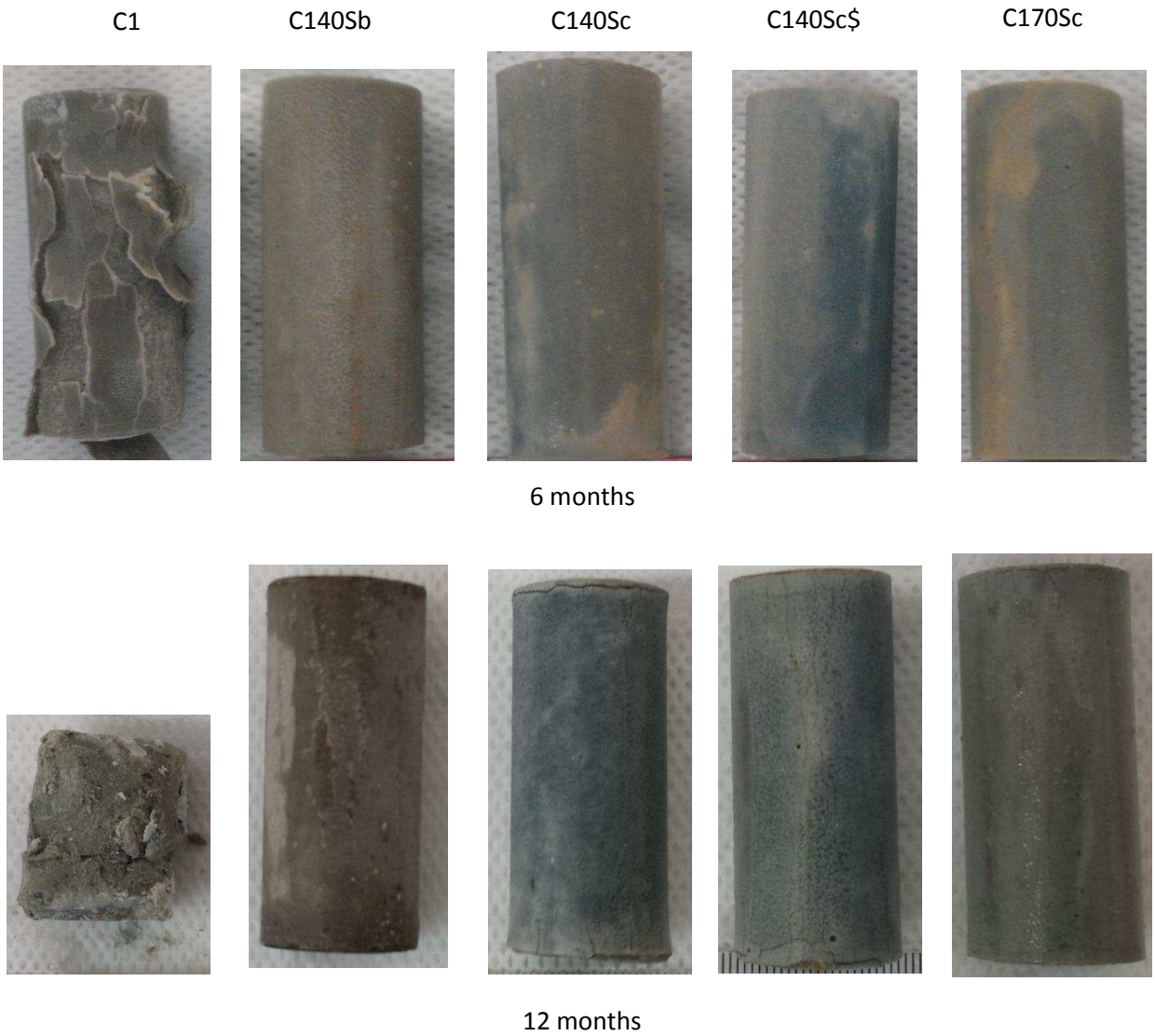

Figure 4 Visual Observations of Pastes Exposed to Na_2SO_4 Attack After 6 and 12 Months

Figure 4 shows the extent of the damage of the pastes exposed to sulfate attack. By 6 months, the neat system had already shown large amounts of scaling on the surface of the cylinders, with initial cracking having been seen after just 2 months of exposure. By 12 months of attack, the sample was very friable and disintegrated readily even with careful handling. The slag blends, however, showed no signs of cracking after 6 months. Some cracking was seen at the top and

bottom ends of the cylinders in pastes $C_1 40 S_c$ and $C_1 40 S_c \$$ only after 12 months of attack, with the extent of damage reduced with the presence of added sulfates.

4.3 Sulfate profile

Figure 5 shows the sulfate profile in pastes after 360 days of curing, measured by EDX analysis. All samples showed a slight increase in the sulfate content close to the surface, rising to a maximum at depths between 0.5 mm and 1 mm depending on the blend. The sulfate content then gradually fell back to background levels with the OPC system showing the greatest penetration depth. The depth at which the maximum sulfate content was seen reduced when using the more reactive slag and with higher slag contents. Also, as the slag content increased, the maximum amount of bound sulfates decreased.

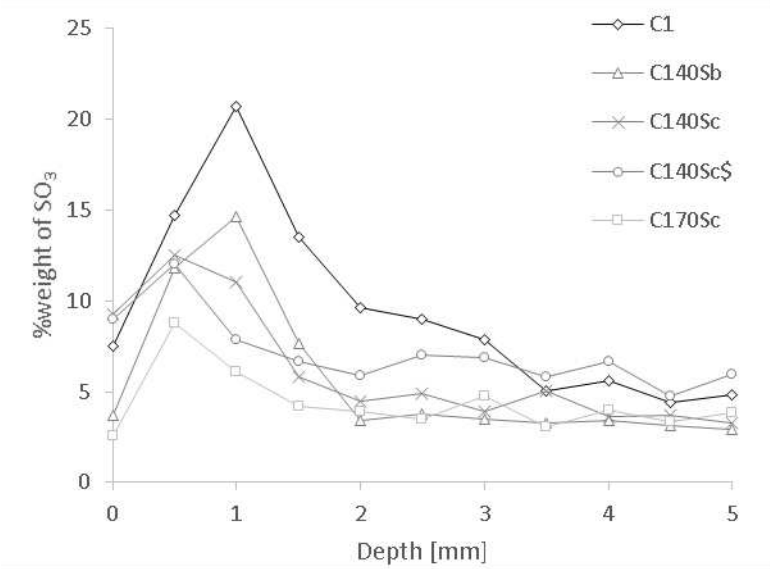

Figure 5 Sulfate Profile Measured on Paste Samples, by SEM-EDX, After 360 days of Curing Exposed to a Sulfate Solution

4.4 Dissolution of the cement clinker and slag

Determination of the phase composition by XRD Rietveld revealed that the kinetics of cement clinker hydration were similar to the reference samples cured under idealized conditions ($Ca(OH)_2$

solution) [33]. Furthermore, slag dissolution did not appear to be exacerbated near the surface, despite the fact that sulfates may promote slag hydration [35]. As such, it was assumed that the degree of hydration of both the clinker and slag fraction in a blend was unaffected during sulfate attack.

4.5 Alumina hydrates

Figure 6 shows the evolution of the ettringite and AFm phases curing in a sulfate laden solution. Before exposure, all samples showed the formation of ettringite with carbonate AFm phases forming within 14 days of hydration (before exposure to sulfates). When exposed to the aggressive media, the ettringite content increased in all systems; with reflections being most intense in the patterns from the neat system and decreasing with slag loading.

Comparing the two mixes with 40 % replacement, the reflections were greatest for the blend containing the aluminium-rich slag (slag C). Additionally analysis of this sample showed the progressive formation of a peak at ~9.8 ° 2Θ, previously observed by Fernandez Altable [21], which could correspond to monosulfate. The sample with additional sulfate showed a similar evolution, however, the increase in the ettringite reflection intensity was less.

The phase evolution was different still in the blend containing higher levels of slag. The increase in intensity of the reflection associated with the ettringite was accompanied by an increase in the intensity of the monosulfate reflection.

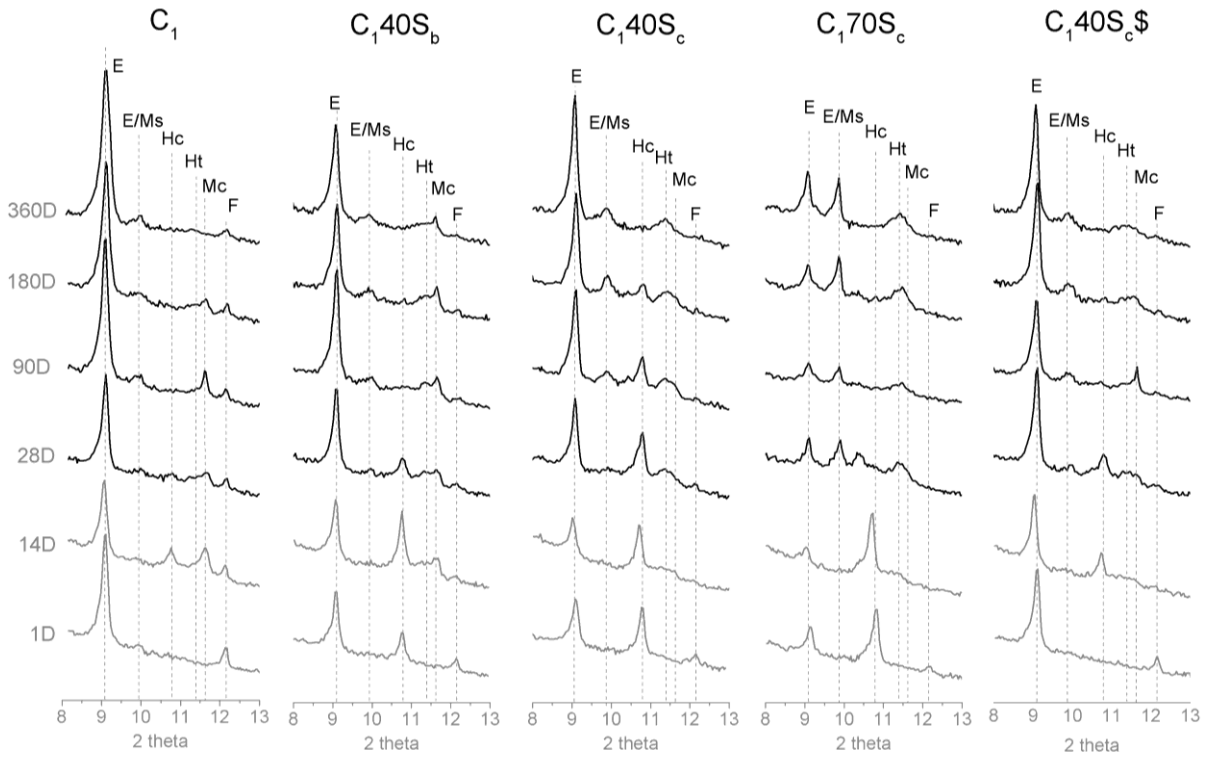

Figure 6 XRD Patterns Obtained from the Outer 1 mm of Pastes Cured for 360 Days in a 3 g.L-1 Na_2SO_4 Solution. The patterns shown in grey are those obtained from samples prior to sulfate exposure. (E - Ettringite, Ms - monosulfate, Hc - Hemicarbonate, Mc - Monocarbonate, Ht – Hydrotalcite, F – C_4AF)

Hydrotalcite formed in all of the slag-cement blends. Traces were seen after 14 days, with levels increasing over time, both for those samples immersed in sulfate solutions (shown) or cured in a Ca(OH)2 solution (not shown). The blends prepared with the magnesium-rich slag C showed more intense reflections, while even stronger reflections were seen with increased slag contents

EDX analysis provided an even greater insight into how the sulfates were bound to the cement hydrates. S/Si v Al/Si plots shown in Figure 7 were obtained after 360 days of curing in a sulfate rich environment from three points; the very surface of the paste samples, at the depth where the greatest amount of sulfate was bound (Figure 5), and at a depth of 5= mm (where the sulfate content was measured to reach background levels).

At the very surface of the samples, there was a cloud of points, representative of the C-A-S-H. The data points lying along the trendline suggest the presence of ettringite in systems C_1, C_140S_b and C_140S_c\$, ettringite and monosulfate in system C_140S_c, and monosulfate in C_170S_c. At the depth where the sulfate content was measured to be the greatest (Figure 5), there was more evidence of ettringite, particularly in samples C_1 and $C140S_b$, while monosulfate was predominant in all the blends prepared with slag C. At background levels, all of the samples showed typical unaffected compositions. Note also that gypsum had formed in samples C_1 and C_140S_b, at depths where the sulfate content was measured to be the highest, as indicated by data points lying above the AFt trendline.

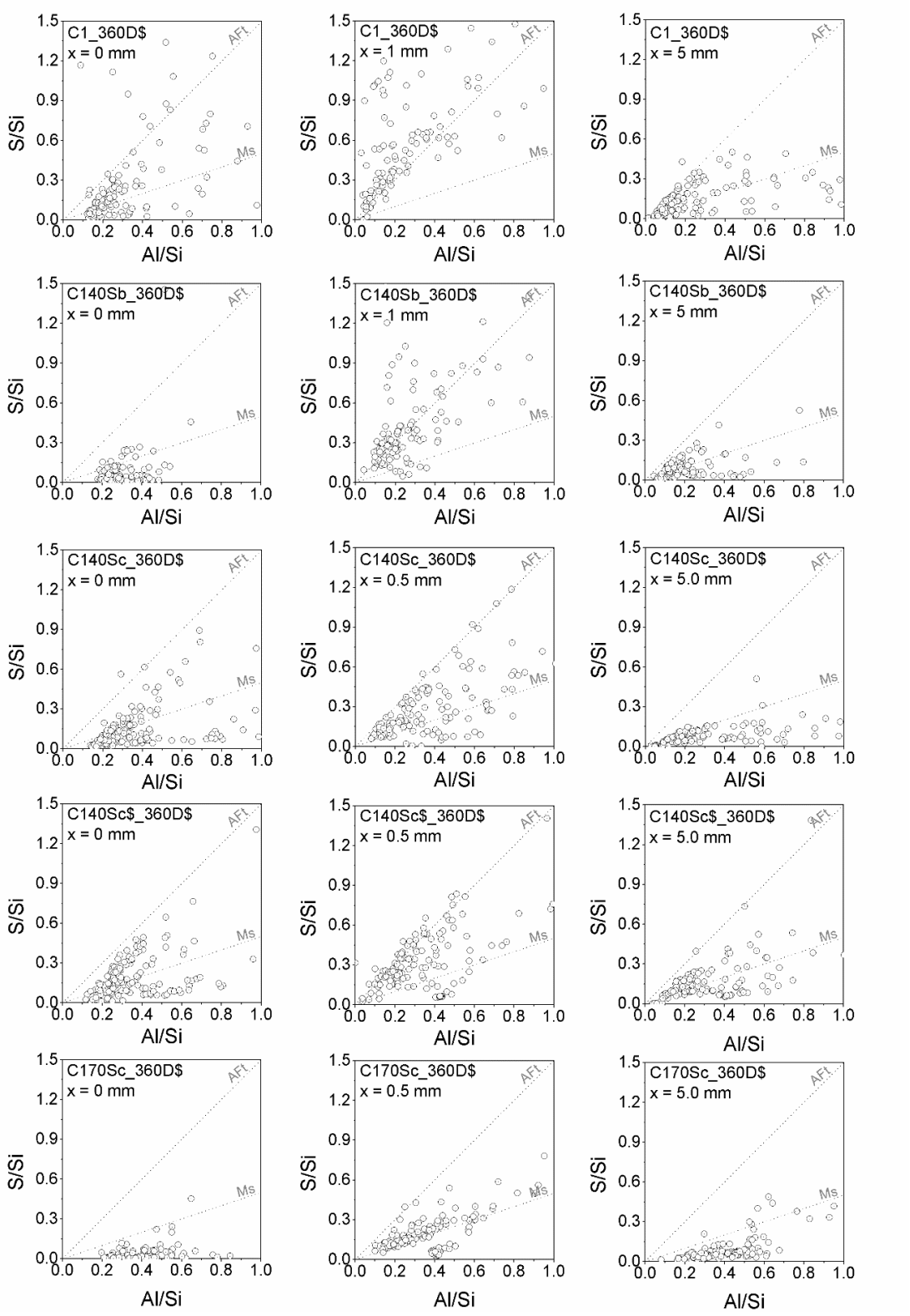

Figure 7 S/Si/ v Al/Si plots for All Systems at Varying Depths Measured by SEM-EDX Analysis (x Denotes Depth, and x = 0 Represents the Measurements Taken Closest to the Surface)

Figure 8 shows the evolution of ettringite, as determined by x-ray diffraction, in the pastes exposed to a sulfate solution, measuring only the outer most 1 mm of the samples (Figure 1). All samples showed an increase in ettringite contents with time; with the neat system C_1 showing both the highest ettringite levels and the greatest increase in ettringite content. As cement was replaced by slag, less ettringite precipitated, both prior to and following immersion in the sulfate solution. At 40% replacement, the blend containing the aluminium-rich slag C yielded slightly more ettringite than that containing slag B; at just over 20%, for blends C_140S_c and $C_140S_c\$$. Very little ettringite precipitated in blend C_170S_c by the end of the testing period. However, this does not reflect the total amount of ettringite possible in this specific blend. The rate of ettringite growth from 14 to 90 days of curing in a sulfate solution in the samples decreased as the slag content increased. C_1 showed the fastest rate of ettringite precipitation, followed by all the samples prepared with 40% slag having compared rates of precipitation and blend C_170S_c showed the lowest rate of ettringite increase. However, this was the only blend where ettringite levels had not reached a plateau in conjunction with the near total consumption of carbonate AFm (Figure 6). Rather, monosulfate had also formed which could potentially convert into ettringite at later ages.

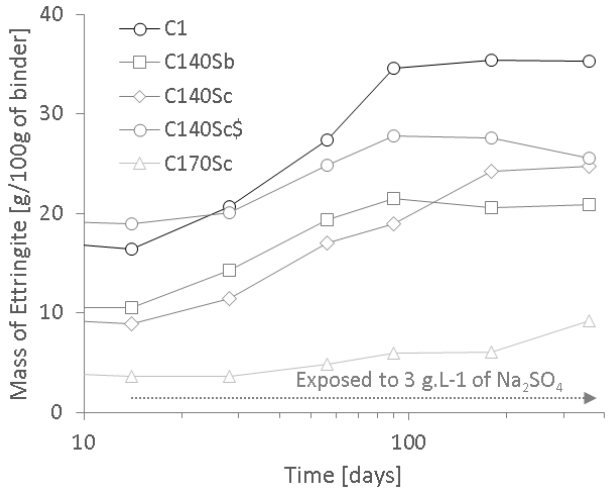

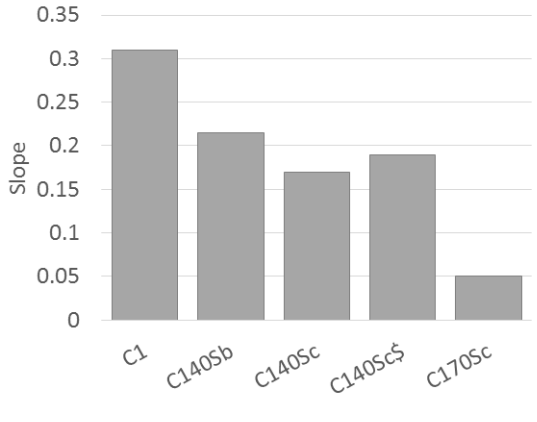

Figure 8 Left: Ettringite Evolution Within the Outer 1 mm (± 2%) in all Pastes Exposed to a Sulfate Solution (Measured by XRD-Rietveld), Right; Slope of the Lines when Linearly Fitting the Points Between 14 and 90 Days.

4.6 Portlandite

Figure 9 shows the calcium hydroxide content from within the outer 1 mm of the pastes subject to attack. The levels of portlandite decreased over time, with it having either leached out of the samples or having been consumed during reactions involving sulfates to produce ettringite, monosulfate, or ultimately gypsum. Depletion was initially very fast, i.e. greater than 50% after just 2 weeks of exposure for all systems, but more gradual thereafter. After 6 months most samples showed just traces of portlandite.

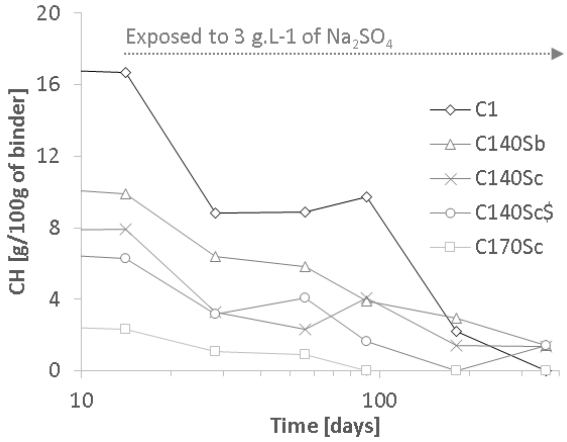

Figure 9 Leaching of Calcium Hydroxide, Measured by TGA, on Pastes Exposed to a Sulfate Solution

4.7 Silica hydrates

Table 4 illustrates the changes in composition of the C-A-S-H phases as a function of depth and time for each sample. The Ca/Si and Al/Si ratios were determined from Al/Ca versus Si/Ca atomic plots and analyzed as described previously [22, 36]; the Al/Si ratios were determined from the slope of the line originating from the origin drawn through the point with the lowest measured

Al/Ca to best avoid intermixing with other phases. The Ca/Si was taken as the point along that same line having the highest Si/Ca ratio.

The slag cements had lower Ca/Si ratios than the neat cement, C_1, typical of slag cements [18, 19], and as previously reported [22]. Upon sulfate exposure, all samples decalcified [37, 38]. In fact, a slight decalcification was observed at the very surface for all the systems after just 2 weeks of exposure to Na_2SO_4. Remarkably, C_1 showed almost no decalcification over the first 6 months of exposure, while the C-A-S-H in all the slag blends had some evidence of decalcification by this point. This is likely due to a buffering effect of portlandite, maintaining the pH of the pore solution high enough to prevent C-A-S-H decalcification. However, by the end of the testing period, the neat system had proportionally decalcified the most, despite the late release of calcium, up to a depth of 1 mm. In all the slag blended systems, decalcification had only occurred to a depth of 0.5 mm.

The aluminium content of the C-A-S-H within the slag cements was higher than in the pure cement system. Exposure to sulfates led to a decrease in Ca/Si ratio [18, 19, 20, 22, 39]. However, there was no evidence of dealumination upon exposure [4, 40, 41], conversely, there was aluminium enrichment at the very edge of the sample.

Table 4 Changes in Ca/Si and Al/Si of the C-A-S-H Phase Measured on Pastes Exposed to a Sulfate Solution, Cured for 360 Days (± 0.05). Reference measurements were taken on samples cured for 28 Days.

depth [x]	Time	C_1		C_140S_b		C_140S_c		C_140S_c\$		C_170S_c	
[mm]	[days]*	Ca/Si	Al/Si	Ca/Si	Al/Si	Ca/Si	Al/Si	Ca/Si	Al/Si	Ca/Si	Al/Si
reference	28	1.81	0.08	1.56	0.11	1.65	0.12	1.61	0.11	1.41	0.15
0	28	1,67	0,05	1,47	0,1	-	-	1,54	0,09	1,35	0,13
	56	1,67	0,06	1,47	0,09	1,62	0,16	1,52	0,14	1,35	0,17
	90	1,67	0,06	1,11	0,1	1,41	0,14	1,41	0,09	1,00	0,21
	180	1,67	0,05	1,12	0,12	-	-	1,26	0,17	0,94	0,23
	360	1	0,13	1,09	0,18	1,05	0,17	1,25	0,15	0,87	0,21
0,5	28	1,72	0,07	1,64	0,07	-	-	1,72	0,09	1,41	0,15
	56	1,78	0,06	1,78	0,09	1,79	0,09	1,69	0,06	1,45	0,16
	90	1,85	0,05	1,78	0,09	1,75	0,09	1,78	0,09	1,39	0,11
	180	1,78	0,05	1,75	0,11	-	-	1,78	0,11	1,47	0,11
	360	1,47	0,04	1,53	0,08	1,61	0,08	1,75	0,11	1,35	0,14
1	28	1,75	0,07	1,61	0,09	-	-	1,72	0,11	1,41	0,13
	56	1,92	0,05	1,72	0,09	1,82	0,09	1,72	0,09	1,45	0,15
	90	1,85	0,05	1,64	0,08	1,69	0,1	1,69	0,09	1,45	0,12
	180	1,79	0,06	1,72	0,09	-	-	1,75	0,12	1,47	0,17
	360	1,72	0,06	1,75	0,09	1,72	0,09	1,78	0,11	1,49	0,13
1,5	28	1,72	0,07	1,61	0,11	-	-	1,79	0,1	1,45	0,16
	56	1,88	0,06	1,72	0,1	1,82	0,09	1,72	0,1	1,45	0,16
	90	1,82	0,06	1,67	0,1	1,72	0,1	1,69	0,09	1,47	0,15
	180	1,75	0,06	1,64	0,1	-	-	1,75	0,11	1,43	0,15
	360	1,85	0,06	1,67	0,09	1,72	0,08	1,75	0,1	1,39	0,17
2	28	1,78	0,06	1,62	0,1	-	-	1,75	0,12	1,47	0,16
	56	1,72	0,05	1,72	0,09	1,75	0,09	1,72	0,1	1,47	0,16
	90	1,79	0,06	1,67	0,09	1,72	0,1	1,78	0,1	1,45	0,16
	180	1,79	0,06	1,64	0,09	-	-	1,75	0,1	1,45	0,16
	360	1,85	0,06	1,64	0,1	1,69	0,09	1,79	0,09	1,47	0,15
5	28	1,78	0,06	1,62	0,09			1,78	0,1		
	56	1,82	0,07	1,67	0,09	1,72	0,11	1,72	0,1	1,49	0,15
	90	1,85	0,05	1,67	0,09	1,72	0,1	1,69	0,1		
	180	1,85	0,05	1,64	0,11			1,72	0,1	1,47	0,16
	360	1,79	0,06	1,67	0,08	1,69	0,09	1,72	0,09	1,43	0,16

* total curing time (sulfate exposure time = total curing time - 14 days)

4.8 Hydrotalcite

Slag hydration leads to the formation of a hydrotalcite-like phase within the hydration rims of the slag grains. Table 5 shows the Mg/Al ratios of the phase formed in each systems. At 180 days, where measurements could be taken along the slag hydration rims with little interference from the hydrated mass, the ratio ranged from 2.67 for blend C_140S_b to 1.93 for blend C_170S_c. Generally more alumina was taken up by hydrotalcite when the alumina was more abundant. The addition of sulfate to a blend led to an increase in Mg/Al ratio, due to alumina being redistributed to form ettringite [22].

After 360 days of curing the ratios had decreased compared to measurements taken after 6 months of curing. A lowering of the Mg/Al with age was previously observed by Taylor et al. [42]. When comparing values taken either near the edge or at the sound core measured after 360 days, lower ratios were measured near the surface.

Table 5 Mg/Al Atomic Ratio of the Hydrotalcite Phase Measured at 180 Days Curing in Ideal Conditions, Serving as Reference, and at 360 Days Curing in a Sulfate Solution with Measurements Taken Near the Surface and at a Depth of 5 mm

	C_140S_b	C_140S_c	C_140S_c\$	C_170S_c
180 Days (lime)	2.67	2.01	2.2	1.93
360 Days (Sulfate, x = 0 mm)	1.98	1.72	2.03	1.66
360 Days (Sulfate, x = 5 mm)	2.11	1.99	1.95	1.78

5 Discussion

5.1 General

As expected the main antagonist of sulfate attack, ettringite, had precipitated at the expense of the carbonate AFm (Figure 6). The amount of ettringite differed between blends, and lowered as the slag content increased (Figure 8). Although the alumina in slag could contribute to AFm formation, its release was limited by slag's lower reactivity and the high Mg/Al of the slag.

Furthermore, in the conversion of AFm to ettringite 2 extra moles of Ca are needed and were likely sourced from calcium hydroxide. In the 40% slag blends, the differences in slag composition (Table 1) and reactivity [1] led to differing ettringite levels. Only a limited amount of ettringite had formed in C_170S_c, the blend richest in alumina. Rather, monosulfate had formed during the testing period (Figure 6). The formation of 'secondary' monosulfate in slag blends exposed to sulfates had been noticed previously [21], and this was confirmed by EDX analysis

figure 7). Even at the depths where the sulfate content was highest, the distribution of the points shifted such that monosulfate was increasingly prevalent as the slag content increased. Ettringite precipitation was rapid during the first 3 months of curing and was much slower thereafter. Interestingly, the rate of ettringite growth decreased as the slag content increased.

Sulfates were also bound with calcium to form gypsum in blends C_1 and C_140S_b only. Several studies have found gypsum formation during sulfate attack, in studies relying on both weakly and strongly concentrated solutions [37, 38, 43, 44, 45, 46, 47]. Whether or not the formation of gypsum can contribute to expansion is often a subject of debate, however, the amounts formed in the aforementioned systems remained minuscule, i.e. undetected by XRD.

5.2 Stability of hydrates

It was seen in Figure 9 that CH levels fell during attack. It was unclear if CH was consumed to form ettringite, or simply leached out into solution, although a distinction was tentatively made in Figure 10. The increase in ettringite levels during attack, when plotted against the CH content, appears to show two stages of reaction. The ettringite content after 14 days of hydration was taken as a zero point. The diagonal grid lines follow the consumption of CH, assuming two moles react with monosulfate to give ettringite. In the first instance (i.e. from the bottom-right of the plot), where the data points draw a line following the slope of the grid lines, it would appear that

CH was most likely consumed to form ettringite, although some leaching of Ca into solution undoubtedly occurred during that stage too. When ettringite was no longer formed during attack, CH was no longer consumed to form ettringite and leaching predominated. This phenomenon was absent in blend C_170S_c due to the very low CH content and the preferential formation of monosulfate in the slag rich system. This suggests that the aluminium found in AFm controls ettringite formation during this stage of attack, consuming the required amount of Ca from CH.

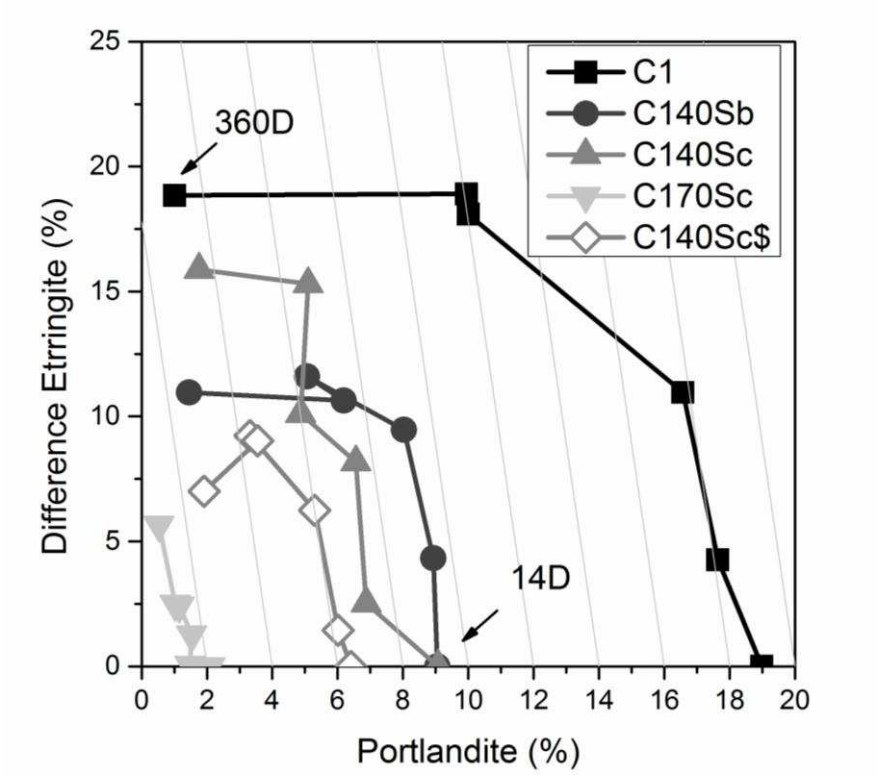

Figure 10 Changes in Ettringite Levels Plotted Against that of CH during Sulfate Attack. Ettringite and CH amounts were estimated by XRD-Rietveld and TGA respectively

The compositional stability of the C-A-S-H phase is shown in Table 4. The C-A-S-H phase proved stable for 180 days of curing in C_1, after which it started to decalcify. In contrast, all the slag blended systems showed earlier onset of decalcification, typically after just 56 or 90 days of curing. This can be explained by the difference in CH contents. The presence of calcium hydroxide buffers the pH to a high enough value to stabilize C-A-S-H. In the slag cement systems, the CH

content was already diluted, and then upon sulfate exposure, depleted with time. The Al/Si of C-A-S-H had increased at the very surface, where the Ca/Si of that same phase had lowered. As such, any availability of aluminium from C-A-S-H to form ettringite can be discounted in neat and slag composite cements.

Much like the C-A-S-H phase, hydrotalcite also appeared to be stable in the presence of sulfates. If anything, the Mg/Al was lower in the attacked zone, indicating a slight uptake of alumina by the phase. This effect was also seen by Komljenović et al. [41] on alkali activated slag (AAS) exposed to sulfate attack. They concluded that sulfate attack had no effect on the structural organization of hydrotalcite. Furthermore, it was observed that the Mg/Al of the phase lowered with higher degrees of hydration (table 5). This was previously seen by Taylor et al. [42]. Consequently, with the C-A-S-H phase and hydrotalcite effectively providing refuge from sulfates for aluminium, any supply of aluminium to promote ettringite formation must come from the slag itself or from AFm phase.

5.3 Mass Balance

In order to confirm the hypothesis that only alumina from AFm phases and dissolving slag may participate in ettringite formation during sulfate attack, a mass balance was performed for all samples cured for 14, 90 and 360 days (see Fig. 11).

After 14 days of curing, alumina was distributed in AFm, AFt, C-A-S-H and hydrotalcite in the neat system. As the sample continued to cure, alumina released by the clinker was primarily used to form AFm, although some was invariably distributed into C-A-S-H and hydrotalcite. This trend was also true in all of the slag blended systems. Furthermore, more alumina was bound to C-A-S-H and hydrotalcite due to a higher Al/Si and Mg content of the C-A-S-H phase and slags respectively. Generally, the overall alumina contents in the slag cements were greater compared

389 to that of C_1 owing to the high alumina content of the slags. The overall alumina content of a slag
390 containing system depended on the composition of the slag and the level of replacement.
391 However, much of the alumina in the slag systems remained in unreacted slag even after a full
392 year of curing. With regards to the AFm contents, only blend C_140S_c had produced more AFm
393 hydrates compared to C_1. This can be explained by the higher reactivity of the slag combined with
394 its high alumina content leading to a higher Al/S ratio in the pore solution promoting AFm growth
395 [22, 29].

396 During sulfate attack, all the alumina in AFm had been consumed in C_1 to form ettringite by 90
397 days. This was also true in blend C_140Sb. However, the situation was different in the blends
398 containing the more alumina-rich slag C. The two blends prepared with 40 % slag C showed only
399 partial conversion of AFm hydrates to ettringite by 90 days. By that time, only blend C_1 showed
400 some damage (Figure 1). The alumina distribution remained generally unchanged from 90 to 360
401 days upon sulfate exposure. However, by this time, blends C_140S_c and $C_140S_c\$$ showed some form
402 of damage, despite no increase in their ettringite contents (Figure 8). For the slag blends,
403 therefore, failure was not due to ettringite growth alone, and another mechanism must have been
404 at play. This is strengthened by the fact that less ettringite had formed in the slag systems,
405 including slag C despite the higher AFm content prior to sulfate attack. This suggests that
406 aluminium is not the only element to be considered. Since additional calcium (from CH) is needed
407 to convert AFm into ettringite (Figure 10), calcium is likely equally important, suggesting that
408 some of the damage may be caused by its leaching in the blended systems.

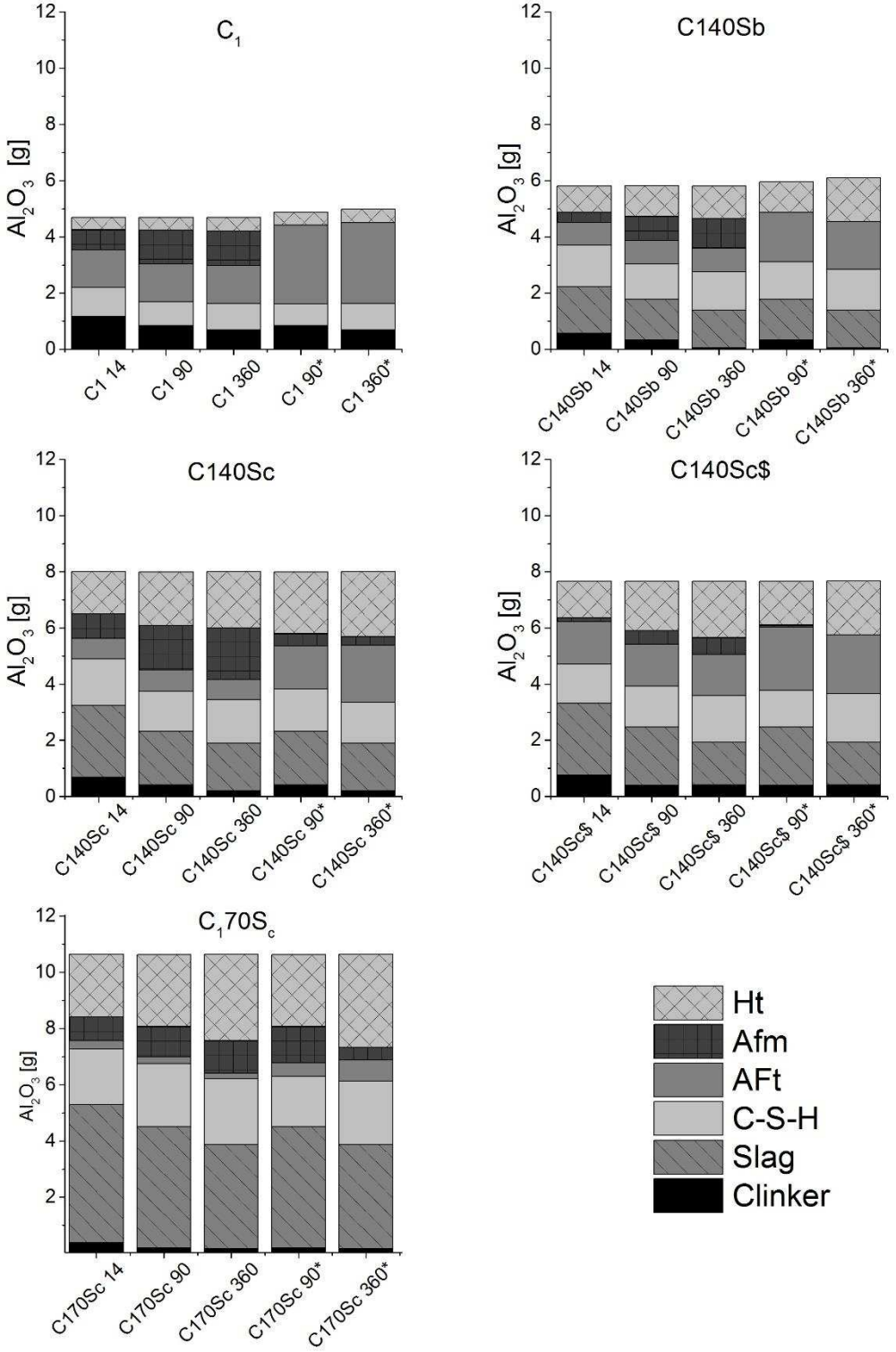

Figure 11 Alumina Distribution after 14, 90 and 360 Days According to Mass Balance. (*) denotes the mass balance for samples curing in $NaSO_4$ solution.

With respect to calcium (Figure 12), much of it was bound to C-A-S-H and CH. During attack, calcium levels in AFm hydrate depleted along with those in CH. To form ettringite from AFm, calcium would have to have been sourced from calcium hydroxide. However, less calcium hydroxide was present in the slag blends, due to dilution of the clinker hydrates and its consumption during slag hydration (Figure 9, Figure 10, at 14 days) [22]. However, the amount available from these phases is unclear as calcium would have also leached out of the samples. In the neat system, much more calcium had been removed from the C-A-S-H phase than in the slag blends (Table 4).

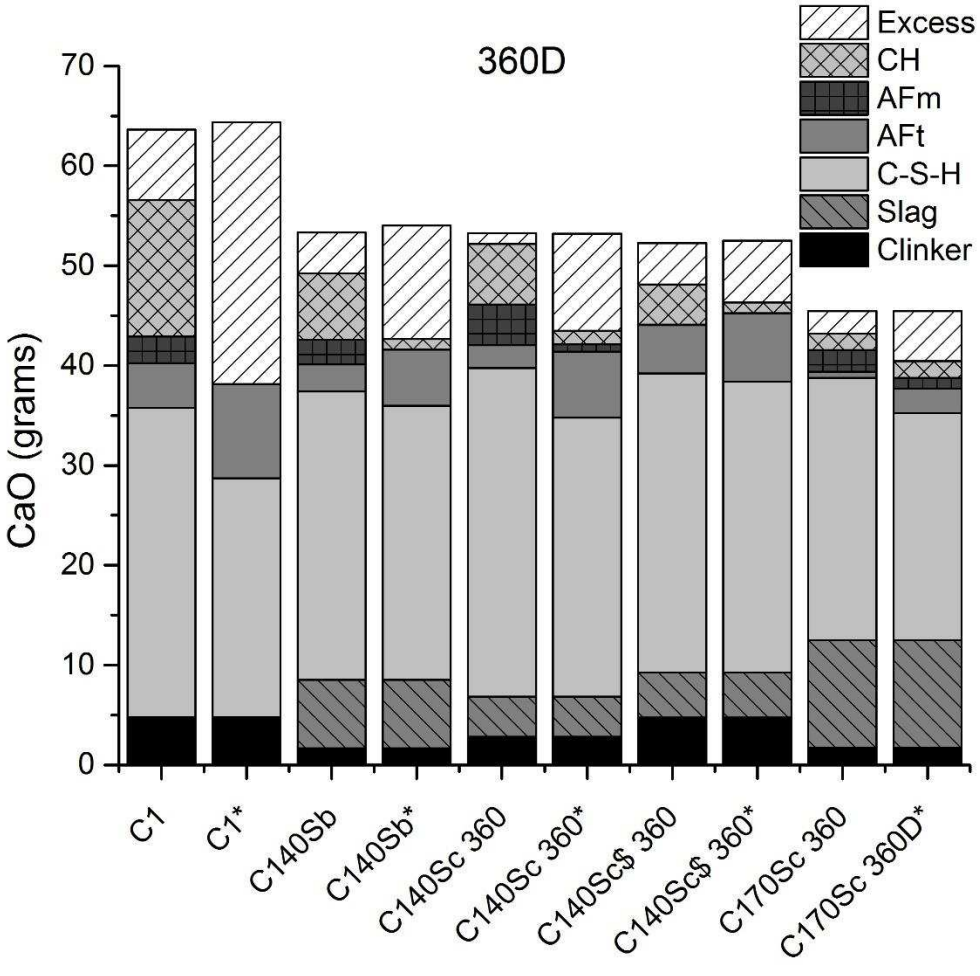

Figure 12 Calcium Distribution after 360 Days of Ideal Curing and After 360 Days of Curing in a Sulfate Solution Estimated by Mass Balance. (*) denotes the mass balance for samples curing in $NaSO_4$ solution.

Consequently, an attempt was made to determine whether the unreacted slag alone could account for ettringite formation upon exposure to sulphate solutions. After 1 year of hydration, all of the clinker phases had hydrated, while residual slag remained [22]. It was assumed that the slag had contributed only to formation of C-A-S-H phase and hydrotalcite. For this exercise, the Ca/Si of the C-A-S-H phase was taken as the average of the 3 measurements 0.0, 0.5 and 1.0 mm (Table 4). For the Al/Si, however, the uptake of alumina was only observed at the very outer layer. Therefore, the Al/Si ratio was taken as the average of the values measured at 0.5 and 1.0 mm. The Mg/Al ratio of the hydrotalcite phase remained unvaried from the values after 1 year of attack (Table 5, 360 days x = 0 mm (sulfate)). The Ca/Si and Al/Si ratios are shown in Table 6.

Table 6 CaO, Al2O3, and MgO Distribution from the Remaining Slag Beyond 1 Year of Hydration [in grams]

	C_140S_b	C_140S_c	$C_140S_c$$	C_170S_c
remaining slag	17.4	12.8	13	28.1
SiO_2 equivalent	7.2	4.5	4.5	9.8
CaO equivalent	6.7	4.9	5	10.8
Al_2O_3 Equivalent	1.3	1.7	1.7	3.7
MgO Equivalent	1.5	1.3	1.3	2.8
C-A-S-H				
Ca/Si	1.46	1.46	1.59	1.24
Al/Si	0.09	0.09	0.11	0.15
CaO demand	9.8 (6.5)	6.1 (4.1)	6.7 (4.1)	11.3 (8.8)
Al_2O_3 demand	0.6	0.3	0.4	1.4
Hydrotalcite				
MgO	1.5	1.3	1.3	2.8
Mg/Al	1.98	1.72	2.03	1.66
Al_2O_3 demand	1.0	0.9	0.8	2.1
Difference				
CaO	**-3.1**	**-1.2**	**-1.7**	**-0.5**
Al_2O_3	**-0.3**	**0.5**	**0.5**	**0.2**

437 In blend C_140S_b, based on EDX analyses, the C-A-S-H phase was determined to have a Ca/Si of
438 1.46. Assuming that all the Si in the remaining anhydrous slag was consumed to form C-A-S-H, the
439 amount of CaO needed to form C-A-S-H with a Ca/Si ratio of 1.46 equated to 9.8 g, more than
440 what can be provided by the slag (6.7 g). Even when assuming an error of $\pm$ 0.05 (1.41<Ca/Si<1.51),
441 the CaO demand varies from 9.5 to 10.1 g. Similarly, the Al/Si was estimated as 0.09, consuming
442 0.6 g of the 1.5 g Al_2O_3 available. Similarly, for the hydrotalcite phase, 1.0 g of Al_2O_3 would be
443 required to maintain the Mg/Al of the phase (1.98 in blend C_140S_b). Combined, the C-A-S-H phase
444 and hydrotalicte would have consumed all of the aluminium released by the slag.

445 Similarly, in the remaining 3 systems prepared with slag C, calcium was never present in sufficient
446 quantities to produce the C-A-S-H phase and maintain the set Ca/Si ratios observed in Table 6.
447 However, the Ca/Si of the C-A-S-H decreases with time in slag blended systems [42]. When
448 comparing the same slag samples after 14 months and 20 years of curing, the Ca/Si of Op C-A-S-
449 H dropped from 1.55 to 1.33 for a blend prepared with 50% slag, and from 1.34 to 1.31 for a blend
450 prepared with 75 % slag [19, 42]. Meanwhile, the C-A-S-H phase in an alkali activated system
451 typically has a Ca/Si of 1 [48]. By recreating the CaO demand of the C-A-S-H assuming a Ca/Si = 1,
452 the CaO demands for all the mixes brackets are obtained. Thus, the CaO demand by the C-A-S-H
453 phase matches much more closely the CaO available in unreacted slags. Evidently, even if the
454 Ca/Si will drop with time, it is most likely that it remain greater than 1. As such it is unlikely that
455 calcium remained available to form ettringite, especially when considering leaching effects after
456 prolonged periods of attack.

457 The alumina demand by the C-A-S-H phase however remained modest in all the systems. Rather,
458 hydrotalcite consumed much of the remaining aluminium. Together with the alumina demand for
459 C-A-S-H formation, little to no alumina was remaining in blends in all the systems. Only, in blends
460 C140Sc and C140Sc$ was alumina in slight excess, However, with a high combined demand of CaO

and Al_2O_3 from C-A-S-H and hydrotalcite, it would appear unlikely that ettringite levels would rise sufficiently for samples to show excessive damage. Rather, calcium would continuously leach over time, leading a loss of strength and decohesion as the C-A-S-H phase is stripped bare from all of its calcium leaving only a silica skeleton.

5.4 Deterioration mechanism

Thermodynamic modelling was used to calculate the saturation indices for ettringite [23] (Figure 13) with the assumption that the C-A-S-H phase is in equilibrium or close to equilibrium with the surrounding pore solution [49].

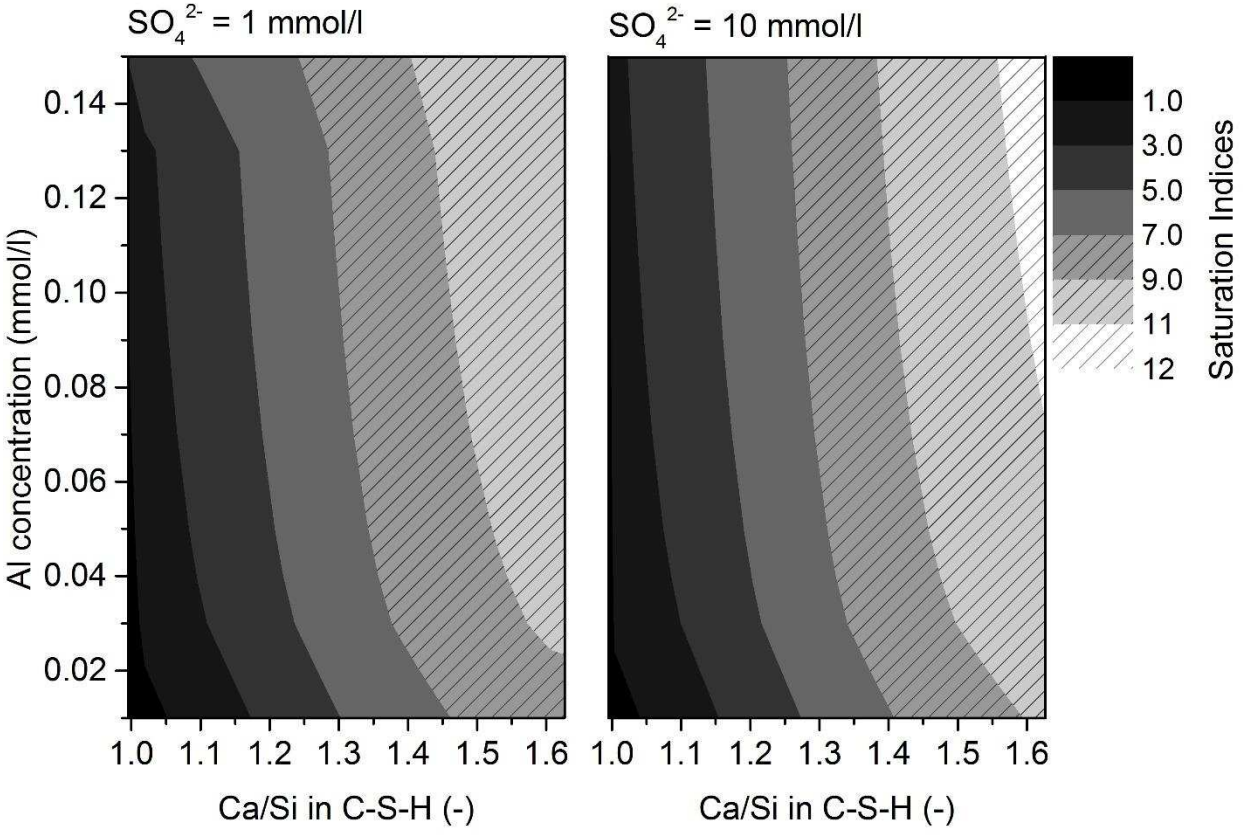

Figure 13 Predicted Saturation Index (SI) of Ettringite (AFt) in a C–S–H Based Model Phase Assemblage

Figure 13 predicts the saturation index (SI) of ettringite (AFt) in a C–S–H based model phase assemblage with increasing Ca/Si ratios and alumina concentration in the pore solution. The saturation index is calculated as $\log(IAP/K_{S0})$, where IAP is the ionic activity product and K_{S0} is the equilibrium solubility product. The area of the plots etched with the diagonal lines show the area where the saturation index of ettringite is limited by solubility of monosulfate and gypsum. In this case the maximum SI of ettringite is close to 7 in log units.

The SI for ettringite increases with increasing Ca/Si ratio of the C–S–H up to Ca/Si = 1.6, above which portlandite buffers the phase assemblage [23, 50]. It is apparent that the calcium ion concentration has an important impact on IAP, as it has the highest exponent apart from water, when compared to sulfate and Al concentrations ($IAP_{AFt} = \{Ca^{2+}\}^6\{Al(OH)_4^-\}^2\{SO4_2^-\}^3\{OH^-\}^4\{H2O\}^{26}$).

At 0.5 mm, the C-A-S-H phase showed a Ca/Si > 1.5 and Al/Si between 0.4 and 1.4 (Table 4) corresponding to alumina concentrations ranging from 0.01 to 0.15 mM/L [49]. At that depth, the S/Si of the C-A-S-H phase varied from 0.08 to 0.15 (see Figure 14), corresponding to SO_4^{2-} concentrations as high as 20 to 40 mmol/L [9, 51]. Consequently, the ettringite should have been strongly supersaturated in the investigated systems, even for the significantly lower sulfate concentration as revealed by modelling (Figure 13). Therefore, the pressure generated from the sulfur species alone would likely exceed the tensile strength of the systems [9] as ettringite formation led to material destruction. However, expansion should be much lower in systems poorer in calcium, with findings that the supersaturation of ettringite decreases in a pore solution being Ca deficient [23].

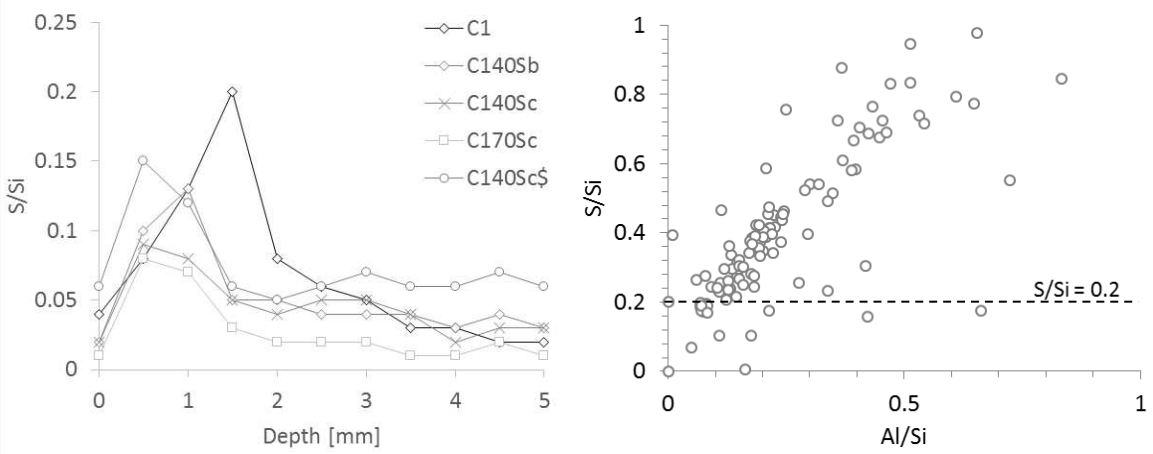

Figure 14 Variation of the S/Si of the C-A-S-H Phase With Depth for All the Investigated Systems. The S/Si ratio is illustrated in the S/Si v Al/Si atomic ratio plot; the minimum S/Si was taken as from the Bottom of the cloud of points

Despite the fact that ettringite was calculated to be strongly supersaturated with regards to sulfur in all systems, ettringite levels did not change significantly after 90 days of curing in a sulfate solution (Figure 8), with the exception of $C_1 40S_c$ which showed remnants of AFm at later ages.

The neat systems was characterized by having the highest AFm and CH content plus having a C-A-S-H richest in Ca. As such, the pore solution was readily saturated with regards to ettringite leading to the most rapid ettringite growth exerting the greatest crystallisation pressure in pores. In response, the pastes were subject to rapid deterioration. By 90 days, AFt levels had reached a plateau and, despite some leaching, still had the greatest amount of CH remaining. The C-A-S-H phase showed minimal leaching by then. C_1 resulted in the system that had formed the greatest amounts of ettringite during attack in a Ca rich system, and was therefore the system whose pore solution was the most supersaturated with regards to ettringite. As a result, the sample showed early signs of cracking from ettringite growth.

In contrast, the slag cements showed much better resistance, with blends $C_1 40S_c$ and $C_1 40S_c$\$ to be the next ones to show appreciable damage, albeit after 12 months of aging in a sulfate solution. However, in all the slag systems containing 40 % slag, ettringite levels had already reached a

513 maximum, or almost, by 90 days. Ettringite levels rose to lower values during attack in the 40 %
514 slag cements when compared to C_1. These systems had less available Al (from AFm), and were
515 more deficient in calcium. Additionally, EDX analysis reveals alumina bound to C-S-H and
516 hydrotalcite were solidly bound to their respective hydrates and, consequently, the solutions
517 were less supersaturated with regards to ettringite (when compared to theoretical calculations).
518 This can only support the idea why slag systems were more resistant.

519 However, by the end of the testing period, the samples still showed some damage. From 90 to
520 360 days, the main changes in microstructure were associated with CH dissolution and C-A-S-H
521 decalcification. Previous studies showed that in response to Ca leaching, porosity and strength of
522 a system increases and decreases respectively [52, 53]. Additionally, leaching of calcium from the
523 C-A-S-H phase, increasingly pronounced after 90 days of curing in a sulfate solution, can lead to
524 significant shrinkage, further increasing porosity and loss of cohesion of the hydrated matrix [54,
525 55]. In systems where ettringite can still be locally supersaturated despite Ca losses, the
526 weakening of the structure could potentially lead to expansion, cracking and spalling.

527 The weakening of the cement paste due to leaching in C_170S_c may be the more likely failing
528 mechanism too. Currently, monosulfate had formed instead of ettringite while CH had fully
529 leached by 90 days of exposure. With Ca continuously being removed and the limited amount of
530 monosulfate, damage by ettringite growth alone is unlikely, and rather Ca leaching is cause of
531 failure in this blend.

532 6 Conclusions

533 Evident differences in microstructure have been observed between a neat cementitious system
534 and slag blend systems. By 14 days of hydration, prior to exposure to external sulfates, neat
535 cement hydrated quickly to produce a C-A-S-H phase rich in calcium and poor in aluminium, plus

AFm hydrates and ettringite. The incorporation of slag led to alumina enrichment in a calcium depleted C-A-S-H phase and a general reduction in AFm contents and, unless calcium sulfate was added, AFt contents. Hydrotalcite had also formed in slag hydration rims, with the quantity formed and the Mg/Al ratio being dependent on the Mg and Al contents of the slags. The work here suggests that a slag rich in Mg may aid resistance to sulfate attack, binding Al to form hydrotalcite. The total porosity of the slag cements was generally greater than that measured in the neat cement, but the porosity was finer.

Only the neat system was readily attacked by sulfates. The addition of slag led to significant improvement in resistance to attack, with blends C_140S_b and C_170S_c being the two most resistant blends. During attack, ettringite levels rose in all the systems, with much of it forming within the first 3 months of attack, during which time carbonate AFm readily supplied alumina. CH was also consumed in the process. However, in the systems using the Al rich slag and containing no additional sulfate, monosulfate had also formed, the levels increasing with the total alumina content of the system. In C_1, C_140S_b and C_140S_c\$, monosulfate contents were absent or below detection levels and gypsum had formed in the 2 former blends. Simultaneously, CH levels dropped dramatically in weeks following exposure to Na_2SO_4 solution. Soon thereafter, C-A-S-H started decalcifying. In response, a sudden increase in alumina content was observed at the very surface of the samples. Hydrotalcite, however, was seen to be relatively stable during attack and, in fact, as hydration progressed, more alumina was bound to this hydrate.

However, ettringite levels in all the systems had reached their near maximum values after 3 months of attack with little to no evolution thereafter. Given the any physical damage to the slag cements was only seen after this time, then ettringite formation alone cannot be the cause of the cracking. With almost all of the cement having hydrated by this time, the only major available source of alumina remaining is therefore the slag. Mass balance calculations showed that there

560 was either insufficient calcium or alumina to generate sufficient ettringite growth in calcium-
561 depleted systems. Slight cracking seen in the slag blends was more likely due to calcium leaching
562 effects opening up the microstructure. Then, in the event that ettringite is locally in
563 supersaturation, cracking may start and propagate.

564 # 7 Acknowledgements

565 This work was funded by a University Research Scholarship from the University of Leeds for Mark
566 Whittaker, with additional funding and materials provided by Heidelberg Technology Centre
567 GmbH. The authors also wish to express their gratitude to Barbara Lothenbach and the referees
568 who provided very constructive feedback.

569

570 # 8 Appendix

571 By adopting a mass balance approach [21, 56], the amount of aluminium and calcium released by
572 the binder components can be tentatively determined and distributed among the hydrates,
573 before and after attack. As such, the role of the main elements involved in damage, forming
574 ettringite, can be distributed following the proposed steps:

575 1. The atomic compositions of the clinker phases and slags, were determined by EDX
576 analysis (table 7). Hydration kinetics were measured by XRD and SEM-BSE image analysis
577 for the clinker and slag fraction respectively, and the amount of each element released
578 was calculated.
579 2. All of the Si was distributed into C-A-S-H and its aluminium and calcium demand
580 was calculated from the Al/Si ratio. For the samples subject to attack, the Ca/Si was taken
581 as an average of the first 1 mm (the degraded zone). Alumina uptake was observed only

at the very surface before regressing rapidly and as such the Al/Si was taken as an average value measured at 0.5 and 1 mm.

3. All of the Mg released was allocated to a hydrotalcite-like phase (Ht). From the Mg/Al of the slag hydration rims, the Al demand was calculated, while a Mg/Al ratio of 2 was assumed for C_1 [48, 57]

4. The ettringite content was experimentally determined by quantitative XRD, and the required Al and Ca demand was subtracted from the remaining content

5. The remaining Al was assumed to be in AFm phases, and the Ca required was calculated. XRD analysis revealed only carbonate AFm, i.e. monocarboaluminate (Mc), as the long term stable AFm hydrate in systems not subjected to sulfate attack [22]. In the attacked samples, monosulfate was considered whose molecular mass is slightly higher compared to Mc and Hc.

6. The CH content was measured by TG, and the subsequent calcium demand calculated. Some Ca invariably remained, and was branded as 'excess'.

Table 7 Atomic Composition of the Clinker Phases

C_3S	$(Ca_{2.900}\,Mg_{0.061}\,Fe_{0.02}\,Na_{0.007}\,K_{0.013})(Al_{0.055}\,Si_{0.940}\,S_{0.003})\,O_{4.959}$
C_2S	$(Ca_{1.950}\,Na_{0.010}\,K_{0.040})(Mg_{0.011}\,Fe_{0.016}\,Al_{0.102}\,Si_{0.898}\,S_{0.006})\,O_{3.971}$
C_3A	$(Ca_{2.972}\,Mg_{0.028}\,Na_{0.016}\,K_{0.027})(Al_{1.628}\,Fe_{0.135}\,Si_{0.216})\,O_{6.006}$
C_4AF	$(Ca_{1.982}Na_{0.006}K_{0.012})(Al_{0.518}Mg_{0.055}Fe_{0.310}Si_{0.117})O_{4.324}$
Slag B	$Ca_{2.524}\,Na_{0.024}\,K_{0.053}\,Si_{2.457}\,Al_{0.539}\,Mg_{0.762}\,S_{0.087}\,O_{9.322}$
Slag C	$Ca_{2.628}\,Na_{0.043}\,K_{0.036}\,Si_{2.212}\,Al_{0.995}\,Mg_{0.931}\,S_{0.139}\,O_{9.948}$

9 Literature

[1] M. WHITTAKER und L. BLACK, „Current Knowledge of External Sulphate Attack," *Advances in Cement Research,* Bd. 27, Nr. 9, pp. 532-545, 2015.

[2] J. MARCHAND und J. P. SKALNY, Materials Science of Concrete: Sulfate Attack Mechanisms, special volume, American Ceramic Society, Ohio, 1999.

[3] J. SKALNY, Materials Science of Concrete III, American Ceramic Society, Ohio, 1992.

[4] R. S. GOLLOP und H. F. W. TAYLOR, „Microstructural and Microanalytical Studies of Sulfate Attack I – Ordinary Portland Cement Paste," *Cement and Concrete Research,* Bd. 22, pp. 1027-1038, 1992.

[5] P. K. MEHTA, „Sulfate Attack on Concrete – A Critical Review," in *Materials Science of Concrete III,American Ceramic Society*, J. SKALNY, Hrsg., 1992, pp. 105-130.

[6] RASHEEDUZZAFAR, O. S. B. AL-AMOUDI, S. N. ABDULJAUWAD und M. MASLEHUDDIN, „Magnesium-Sodium Sulfate Attack in Plain and Blended Cements," *Journal of Materials in Civil Engineering,* Bd. 6(, Nr. 2, pp. 201-222, 1994.

[7] B. LOTHENBACH, B. BARY, P. LE BESCOP, T. SCHMIDT und N. LETERRIER, „Sulfate Ingress in Portland Cement," *Cement and Concrete Research,* Bd. 40, pp. 1211-1225, 2010.

[8] W. KUNTHER, B. LOTHENBACH und K. L. SCRIVENER, „On the Relevance of Volume Increase for the Length Changes in Mortar Bars in Sulfate Solution," *Cement and Concrete Research,* Bd. 46, pp. 23-29, 2013.

[9] C. YU, W. SUN und K. SCRIVENER, „Mechanism of Expansion of Mortars Exposed in Sodium Sulphate Solutions," *Cement and Concrete Research,* Bd. 43, pp. 105-111, 2013.

[10] W. MULLAUER, R. E. BEDDOE und D. HEINZ, „Sulfate Attack Expansion Mechanisms," *Cement and Concrete Research,* Bd. 52, pp. 208-215, 2013.

[11] G. W. SCHERER, „Stress from Crystallisation of Salt," *Cement and Concrete Research,* Bd. 34, pp. 1613-1624, 2004.

[12] C. YU, W. SUNB and K. SCRIVENER, "Degradation mechanism of slag blended mortars immersed in sodium sulfate solution," *Cement and Concrete Research,* vol. 72, p. 37–47, 2015.

[13] D. D. HIGGINS, „Increased Sulfate Resistance of GGBS Concrete in the Presence of Carbonate," *Cement and Concrete Composites,* Bd. 25, Nr. 8, pp. 913-919, 2003.

[14] R. S. GOLLOP und H. F. W. TAYLOR, „Microstructural and Microanalytical Studies of Sulfate Attack, V, Comparison of Different Slag Blends," *Cement and Concrete Research,* Bd. 27, pp. 1029-1044, 1996.

[15] S. OGAWA, T. NOZAKI, K. YAMADA, H. HIRAO und R. D. HOOTON, „Improvement on Sulfate Resistance of Blended Cement with High Alumina Slag," *Cement and Concrete Research,* Bd. 42, pp. 244-251, 2012.

[16] R. D. HOOTON und J. J. EMERY, „Sulfate Resistance of a Canadian slag Cement," *ACI Materials Journal,* Bd. 87, Nr. 6, pp. 547-555, 1990.

[17] F. W. LOCHER, „The Problem of the Sulfate Resistance of Slag Cements," *Zement-Kalk-Gibs (Weisbaden),* Bd. 9, pp. 395-401, 1966.

[18] I. G. RICHARDSON, „The nature of C–S–H in hardened cements," *Cement and Concrete Research,* Bd. 29, p. 1131–1147, 1999.

[19] I. G. RICHARDSON und G. W. GROVES, „Microstructure and Microanalysis of Hardened Cement Pastes Involving Ground Granulated Blast-Furnace Slag," *Journal of Material Science,* Bd. 27, pp. 6204-6212, 1992.

[20] I. G. RICHARDSON und G. W. GROVES, „The structure of the calcium silicate hydrate phases present in hardened pastes of white Portland cement blast-furnace slag blends," *Journal of Materials Science,* Bd. 32, Nr. 18, p. 4793–4802, 1997.

[21] V. FERNANDEZ-ALTABLE, Availability of Al2O3 in Slag Blended Cements: Sulphate Attack Implications, Final Conference of the NANOCEM Marie Curie Research Training Network, Villars-sur-Ollon, September 1-3, 2009.

[22] M. WHITTAKER, M. ZAJAC, M. BEN HAHA, F. BULLERJAHN und L. BLACK, „The Role of the Alumina Content of Sag, Plus the Presence of Additional Sulfate on the Hydration and Microstructure of Portland cement-Slag Blends," *Cement and Concrete Research,* Bd. 66, 2014.

[23] W. KUNTHER, B. LOTHENBACH und J. SKIBSTED, „Influence of the Ca/Si ratio of the C-S-H Phase on the Interaction with Sulfate Ions and its Impact on the Ettringite Crystallisation Pressure," *Cement and Concrete Research,* Bd. 69, pp. 37-49, 2015.

[24] D. JANSEN, F. GOETZ-NEUNHOEFFER, C. STABLER und J. NEUBAUER, „A Remastered External Standard Method Applied to the Quantification of Early OPC hydration," *Cement and Concrete Research,* Bd. 41, pp. 602-608, 2011.

[25] D. KULIK, GEMS 2, software, http://gems.web.psi.ch/ PSI, Villigen, Switzerland,, 2010.

[26] W. HUMMEL, U. BERNER, E. CURTI, F. J. PEARSON und T. THOENEN, Nagra/PSI chemical thermodynamic data base 01/01, Universal Publishers/uPUBLISH.com, USA also published as Nagra Technical Report NTB 02-16, Wettingen, Switzerland, 2002.

[27] T. THOENEN und D. KULIK, Nagra/PSI chemical thermodynamic database 01/01 for GEMS-selektor (V.2-PSI) geochemical modelling code, http://gems.web.psi.c/doc/pdf/TM-44-03-04-web.pdf PSI, Villigen, 2003.

[28] B. LOTHENBACH und F. WINNEFELD, „Thermodynamic modelling of the hydration of Portland cement," *Cement and Concrete Research,* Bd. 36, p. 209–226, 2006.

[29] T. MATSCHEI, B. LOTENBACH und F. P. GLASSER, „Thermodynamic properties of Portland cement hydrates in the system CaO–Al2O3–SiO2–CaSO4–CaCO3–H2O," *Cement and Concrete Research,* Bd. 37, p. 1379–1410, 2007.

[30] B. LOTHENBACH, T. MATSCHEI, G. MOSCHNER und F. P. GLASSER, „Thermodynamic modelling of the effect of temperature on the hydration and porosity of Portland cement," *Cement and Concrete Research,* Bd. 38, p. 1–18, 2008.

[31] K. L. SCRIVENER, H. H. PATEL, P. L. PRATT und L. J. PARROTT, „Analysis of Phases in Cement Paste Using Backscattered Electron Images, Methanol Adsorption and Thermogravimetric Analysis," *Materials Research Society Symposium Proceedings,* Bd. 85, pp. 67-76, 1987.

[32] K. L. SCRIVERNER, „Backscattered Electron Imaging of Cementitious Microstructures: Understanding and Quantification," *Cement and Concrete Composites,* Bd. 26, pp. 935-945, 2004.

[33] MarkWhittaker, M. Zajac, M. B. Haha, F. Bullerjahn und L. Black, „The role of the alumina content of slag, plus the presence of additional sulfate on the hydration and microstructure of Portland cement-slag blends," *Cement and Concrete Research,* Bd. 66, pp. 91-101, 2014.

[34] J. BIJEN, „Benefits of Slag and Fly Ash," *Construction of Building Materials,* Bd. 10, Nr. 5, pp. 309-314, 1996.

[35] M. WHITTAKER, „The Impact of Slag Composition on the Microstructure of Composite Slag Cements Exposed to Sulfate Attack.," *PhD Thesis, University of Leeds,* 2014.

[36] F. DESCHNER, F. WINNEFELD, B. LOTHENBACH, S. SEUFERT, P. SCHWESIG, S. DITTRICH, F. GOETZ NEUNHOEFFER und J. NEUBAUER, „Hydration of Portland Cement with High Replacement by Siliceous Fly Ash," *Cement and Concrete Research,* Bd. 42, pp. 1389-1400, 2012.

[37] D. PLANEL, J. SERCOMBE, P. LE BESCOP, F. ADENOT und J.-M. TORRENTI, „Long-Term Performance of Cement Paste During Combined Calcium Leaching-Sulfate Attack: Kinetics and Size Effect," *Cement and Concrete Research,* Bd. 36, pp. 137-143 , 2006.

[38] R. EL-HACHEM, E. ROZIERE, F. GRONDIN und A. LOUKILI, „New Procedure to Investigate External Sulphate Attack on Cementitious Materials, Cement and Concrete Composites," Bd. 34, pp. 357-364, 2012.

[39] P. FAUCON, A. DELAGRAVE, J. C. PETIT, C. RICHET, J. M. MARCHAND und H. ZANNI, „Aluminium Incorporation in Calcium Silicate Hydrates (C-S-H) Depending on their Ca/Si Ratio," *Journal of Physical Chemistry B,* Bd. 103, Nr. 37, pp. 7796-7802, 1999.

[40] D. HEINZ, W. MULLAUER und R. E. BEDDOE, „Mechanismen des Sulfatangriffs auf Beton - Aspekte des Chemischen und Physikalischen Widerstands," in *Ibausil*, Weirmar, 2012.

[41] M. KOMLJENOVIĆ, Z. BAŠČAREVIĆ, N. MARJANOVIĆ und V. NIKOLIĆ, „External Sulfate Attack on Alkali-Activated Slag," *Construction and Building Materials,* Bd. 49, pp. 31-39, 2013.

[42] R. TAYLOR, R. G. RICHARDSON und R. M. D. BRYDSON, „Composition and Microstructure of 20-year-old Ordinary Portland-Ground Granulated Blast-Furnace Slag Blends Containing 0 to 100% Slag," *Cement and Concrete Research,* Bd. 40, pp. 971-983, 2010.

[43] B. TIAN und M. D. COHEN, „Does Gypsum Formation During Sulphate Attack on Concrete Lead to Expansion," *Cement and Concrete Research,* Bd. 30, pp. 117-123, 2000.

[44] J. G. WANG, „Sulfate Attack on Hardened Cement Paste," *Cement and Concrete Research,* Bd. 24, pp. 735-742, 1994.

[45] M. A. GONZALEZ und E. F. IRASSAR, „Ettringite Formation in Low C3A Portland Cement Exposed to Sodium Sulfate Solution," *Cement and Concrete Research,* Bd. 27, pp. 1061-1072, 1997.

[46] M. SANTHANAM, M. D. COHEN und J. OLEK, „Effects of Gypsum Formation on the Performance of Cement Mortars During External Sulfate Attack," *Cement and Concrete Research,* Bd. 33, pp. 325-332, 2003.

[47] A. CHABRELIE, Mechanisms of Degradation of Concrete by External Sulfate Ions Under Laboratory and Field Conditions, PhD Thesis, EPFL, 2010.

[48] M. BEN HAHA, B. LOTHENBACH, G. LE SAOUT und F. WINNEFELD, „Influence of the Slag Chemistry on the Hydration of Alkali-Activated Blast-Furnace Slag – Part II: Effect of Al2O3," *Cement and Concrete Research,* Bd. 42, pp. 74-83, 2012.

[49] B. LOTHENBACH und A. NONAT, „Calcium Silicate Hydrates: Solid and Liquid Phase Composition," *Cement and Concrete Research,* Bd. 78 (part A), pp. 57-70, 2015.

[50] D. A. KULIK und M. KERSTEN, „Aqueous Solubility Diagrams for Cementitious Waste Stabilization Systems: II, End-Member Stoichiometries of Ideal Calcium Silicate Hydrate Solid Solution," *Journal of the American Ceramic Society,* Bd. 84, Nr. 12, pp. 3017-3026, 2001.

[51] R. BARBARULO, „Comportement des Materiaux Cimentaires: Actions des Sulfates et de la Temperature," *PhD Thesis,* p. Ecole Superieure de Cachan, 2002.

[52] Y. S. CHOI und E. I. YANG, „Effect of Calcium Leaching on the Pore Structure, Strength, and Chloride Penetration Resistance in Concrete Specimens," *Nuclear Engineering and Design,* Bd. 259, pp. 126-136, 2013.

[53] W. LIN, A. CHENG, R. HUANG, C. CHEN und X. ZHOU, „Effect of Calcium Leaching on the Properties of Cement-Based Composites," *Journal of Wuhan University of Technology Materials Science,* Bd. 26, Nr. 5, pp. 990-997, 2011.

[54] J. J. CHEN, J. J. THOMAS und H. M. JENNINGS, „Decalcification Shrinkage of Cement Paste," *Cement and Concrete Research,* Bd. 36, Nr. 5, pp. 801-809, 2006.

[55] M. AUROY, S. POYET, P. LE BESCOP, J. M. TORRENTI, T. CHARPENTIER, M. MOSKURA und X. BOURDON, „Impact of Carbonation on Unsaturated Water transport Properties of Cement-Based Materials," *Cement and Concrete,* Bd. 74, pp. 44-58, 2015.

[56] H. W. F. TAYLOR, Cement Chemistry, London: Academic Press Limited, 1992.

[57] J. S. LUMLEY, R. S. GOLLOP, G. K. MOI und H. F. W. TAYLOR, „ Degrees of Reaction of the Slag in Some Blends with Portland Cements," *Cement and Concrete Research,* Bd. 26, pp. 139-151, 1996.

600

601

602